Characterizing the Impacts of Rice Fading on a WiFi-based Passive Multistatic Radar Using Cramer-Ráo Bound

Muhammad Nohman Javed, Syed Ali Hassan and Sajid Ali
School of Electrical Engineering and Computer Science (SEECS)
National University of Sciences and Technology (NUST), Islamabad, Pakistan
Email: {13mseemjaved, ali.hassan, sajid.ali}@seecs.edu.pk

***Abstract*—In this paper, the performance of a WiFi-based passive multistatic radar is studied in a Rice fading (RF) environment, where the received signal from the target is composed of fixed amplitude or dominant scatterer (DS) component and weak isotropic scatterers (WIS) component. The likelihood expression of the received signal is derived and modified Cramer-Rao lower bound (MCRLB) expressions for 3D Euclidean components of target position and velocity are computed. It is shown that in presence of RF, the total modified Fisher information matrix (MFIM) is a linear combination of MFIM due to WIS and DS components. With the help of numerical examples, it is established that existence of DS component increases target radar cross section (RCS), which improves the detection and estimation accuracy. It is also shown that by exploiting DS, the performance of a waveform can be analyzed for generalized radar cross section model (GRCSM), which shows its characterization for various radar applications.**

***Index Terms*—WiFi, Cramer-Rao bounds, Rice fading, multistatic, passive radar, radar cross section, Swerling target.**

I. Introduction

Passive radar is a type of bistatic radar that utilizes signals from broadcast and communication sources for various radar application purposes. These sources are known as illuminator of opportunities and include signals such as FM signal, digital audio & video broadcast (DAB & DVB), cellular signals for instance, universal mobile telecommunication system (UMTS), 4G long term evolution (LTE), among others. Besides many other advantages [1], passive radar operate in a multistatic configuration provides spatial and frequency diversity, which tends to increase the accuracy of target's detection and estimation of its various parameters.

Over the recent years, regular availability of WiFi transmission makes it a potential illuminator of opportunity for various local area indoor [2] and outdoor [3] applications. Falcone, et al. in [4], discusses in detail the potentialities and challenges in WiFi-based passive radar. Many researchers have conducted experimental studies [3], while other properties such as multipath impacts [5] and localization issues [2] are also studied.

In this paper, we evaluate the performance of an IEEE 802.11b (WiFi)-based passive multistatic radar in a Rice fading (RF) environment, where dominant scatterer (DS) components are available along with the weak istropic scatterers (WIS) components from a target. We compute the modified Cramer-Rao lower bounds (MCRLB) on 3D Euclidean components of target's position and velocity. The main motivation behind this study is two-folds.

Firstly, WiFi has very low transmitting power with the effective isotropic radiated power (EIRP) of less than one Watt. This power is usually inadequate for accurate detection of target and accuracy of estimation reduces in the presence of strong clutters, direct signal interference (DSI) and other unwanted signals. Since, the transmit power is not in control of passive receiver designer, the required reflected power from the target can be increased by exploiting DS along with WIS. With the aid of multistatic geometry, it is possible to obtain DS on some receivers in both less scattering outdoor and rich scattering indoor environment by exploiting statistical DS detection schemes such as LiFi [6]. The presence of DS component increases target radar cross section (RCS), which results in increase in the signal-to-noise (SNR) ratio at the receiver. Consequently, the performance of detection and estimation improves.

On the other hand, the target RCS varies with variation in aspect angle, frequency and polarization. With the exploitation of DS and WIS together, a performance of waveform can be evaluated for different RCS models that appear in different radar applications. In this study, we use Rician target model which approximates a broad range of famous Swerling $0-V$ target models defined as generalized radar cross section model (GRCSM) in [7]. Thus a unified framework is provided to evaluate the performance of a waveform analytically for Swerling models and performance limits are given in the form of MCRLBs expressions. Also performance limits can be evaluated when target RCS observes different for different transceiver pairs, which is helpful to evaluate performance limits with multiple targets.

The rest of the paper is structured as follows. The signal model is proposed in Section II. The computation of MCRLBs is given in Section III and its numerical evaluation is given in Section IV, respectively. Finally, Section V concludes the paper.

978-1-5090-0863-6/16/$31.00 ©2016 IEEE

II. SIGNAL MODEL

Consider a multistatic geometry in a 3D Euclidean space having M_T transmitters, M_R receivers and a single target. Let the transmitters and receivers are positioned at $\mathbf{T}_i = (t_{x_i}, t_{y_i}, t_{z_i})$ and $\mathbf{R}_j = (r_{x_j}, r_{y_j}, r_{z_j})$, where $i = [1, 2, ..., M_T]$ and $j = [1, 2, ..., M_R]$, respectively. Let the position and velocity of the target are represented as $\mathbb{T}_p = (p_x, p_y, p_z)$ and $\mathbb{T}_v = (v_x, v_y, v_z)$, respectively. The signal transmitted by the i^{th} transmitter will be given as

$$u_i(t) = \frac{1}{\sqrt{N}} \sum_{n=0}^{N-1} c_{in} g_i\left(t - nT\right), \tag{1}$$

where, c_{in} is the transmitted symbol which may be either binary or quadrature phase shift keying (BPSK or QPSK) symbol depending upon frame type and data rate, N is total number of symbols and T is the symbol time. The $g_i(t) = h_i(t - \frac{D}{2})$ is the delayed root-raised cosine (RRC) pulse, where D is picked out such that $\int_{-D/2}^{D/2} h^2(t)dt \leq 1$. By using the orthogonality of an RRC pulse under T-shifts, we have

$$\begin{cases} \int_{-\infty}^{\infty} g_i\left(t - nT\right) g_i\left(t - kT\right) = 0, \forall\, n \neq k \\ \int_{-\infty}^{\infty} g_i\left(t - nT\right) g_i\left(t - kT\right) = \int_{-\infty}^{\infty} h^2(t)dt = 1, \forall\, n = k. \end{cases} \tag{2}$$

Due to wide separation among the antennas, it is reasonable to assume that each transceiver pair has independent aspect angle for the target and thus has independent attenuation coefficient. Furthermore, we assume that signals from different transmitters at each receiver are separable in some orthogonal domain as per [8]. Using the Rician target model, the signal received at the j^{th} receiver from the i^{th} transmitter will be

$$y_{ij}(t) = \beta_{ij} u_i(t - \tau_{ij}) e^{-j2\pi f_{D_{ij}}(t - \tau_{ij})} + w_{ij}(t), \tag{3}$$

where β_{ij} is the attenuation or reflection coefficient. Being composed of a DS and many independent WIS, it is modeled as a complex Gaussian random variable with mean m_{ij} and variance σ^2, i.e., $\beta_{ij} \sim CN(m_{ij}, \sigma^2)$. The $w_{ij}(t)$ is the the additive white Gaussian noise with zero mean and variance σ_n^2 i.e., $w_{ij} \sim CN(0, \sigma_n^2)$, independent to β_{ij}. The parameters m_{ij}, σ^2 and σ_n^2 are considered to be deterministic and known. The terms τ_{ij} and $f_{D_{ij}}$ are the delay and doppler shift associated with $i - j^{th}$ path given as

$$\tau_{ij} = \frac{|\mathbf{T}_i \mathbb{T}_p| + |\mathbf{R}_j \mathbb{T}_p|}{c}, \tag{4}$$

$$f_{D_{ij}} = \frac{(\mathbb{T}_p \mathbf{R}_j) \cdot \mathbb{T}_v}{\lambda |\mathbf{R}_j \mathbb{T}_p|} + \frac{(\mathbb{T}_p \mathbf{T}_i) \cdot \mathbb{T}_v}{\lambda |\mathbf{T}_i \mathbb{T}_p|}, \tag{5}$$

where λ is the carrier wavelength, c is the speed of light, $|\mathbf{T}_i \mathbb{T}_p|$ and $|\mathbf{R}_j \mathbb{T}_p|$ are the Euclidean distances from the i^{th} transmitter to the target and from the target to the j^{th} receiver, respectively. The $|\mathbf{T}_i \mathbb{T}_p|$ and $|\mathbf{R}_j \mathbb{T}_p|$ are given as

$$|\mathbf{T}_i \mathbb{T}_p| = \sqrt{(p_x - t_{x_i})^2 + (p_y - t_{y_i})^2 + (p_z - t_{z_i})^2}, \tag{6}$$

$$|\mathbf{R}_j \mathbb{T}_p| = \sqrt{(p_x - r_{x_j})^2 + (p_y - r_{y_j})^2 + (p_z - r_{z_j})^2}. \tag{7}$$

Now the conditional likelihood of a single transmitter-receiver pair is derived by using the concepts given in [9], the logarithm of which for a given transmitted symbol $\mathbf{c}$, is written as

$$\begin{aligned} &\log \wedge(y_{ij}(t)|\mathbf{c}) = \\ &\frac{\sigma^2}{\sigma_n^2 + \sigma^2} \left| \int_{-\infty}^{\infty} y_{ij}(t) u_i^*(t - \tau_{ij}) e^{-j2\pi f_{D_{ij}}(t - \tau_{ij})} dt \right|^2 - \\ &\frac{1}{\sigma^2 + \sigma_n^2} \left| \int_{-\infty}^{\infty} m_{y_{ij}} u_i^*(t - \tau_{ij}) e^{-j2\pi f_{D_{ij}}(t - \tau_{ij})} dt \right|^2 + \\ &\frac{2}{(\sigma^2 + \sigma_n^2)} \Re\Bigg(\int_{-\infty}^{\infty} y_{ij}(t) u_i^*(t - \tau_{ij}) e^{-j2\pi f_{D_{ij}}(t - \tau_{ij})} dt \times \\ &\int_{-\infty}^{\infty} m_{y_{ij}}^* u_i(t - \tau_{ij}) e^{j2\pi f_{D_{ij}}(t - \tau_{ij})} dt \Bigg) + \ln\left(\frac{\sigma_n^2}{\sigma_n^2 + \sigma^2}\right), \end{aligned} \tag{8}$$

where $|.|$ is the absolute operator, $(.)^*$ is the conjugation operator, $\Re(.)$ is the real part and $m_{y_{ij}} = m_{ij} u_i(t - \tau_{ij}) e^{j2\pi f_{D_{ij}}(t - \tau_{ij})}$ is the mean of the received signal $y_{ij}(t)$. The joint likelihood over $M_T \times M_R$ independent transceiver pairs is the product of all single transceiver pair likelihoods. Therefore, the joint log likelihood is the sum of individual log likelihoods and is given by

$$\log \Lambda(\mathbf{y}(t)|\mathbf{c}) = \sum_{i=1}^{M_T} \sum_{j=1}^{M_R} \log \wedge\left(y_{ij}(t)|\mathbf{c}\right). \tag{9}$$

III. MCRLB EVALUATION

CRLBs are widely used to determine the lower bounds on the local estimation accuracy of the unbiased estimators. In this study, we use the MCLRB in which the expectation is taken over the conditional likelihood of the received data conditioned on the transmitted symbols. This is unlike to the classical CRLB, in which average is taken over the joint likelihood of the received signal and transmitted symbols. The classical CRLB is infeasible for this study due to randomness of the data [10]. The situations where CRLB is not applicable , the MCRLB is easier to calculate and is considered to be a good performance indicator. To evaluate MCRLB, we first need to compute the modified Fisher information matrix (MFIM) on parameters $\mathbf{\Phi} = [\tau_{ij}, f_{D_{ij}}]\ \forall\ i, j$. For this, we first write the expression in (8) in a simplified form as

$$\log \Lambda(\mathbf{y}; \mathbf{\Phi}|\mathbf{c}) = \sum_{i=1}^{M_T} \sum_{j=1}^{M_R} \left(\Gamma_{ij} - \Pi_{ij} + \Sigma_{ij}\right) + \ln C, \tag{10}$$

where Γ_{ij}, Π_{ij} and Σ_{ij} are the first, second and third terms in (8), respectively and $C = \sigma_n^2/(\sigma_n^2 + \sigma^2)$. For a single transceiver pair, the MFIM $\mathbf{F}_{ij}^{\mathbf{y}}(\mathbf{\Phi})$, by definition is given as

$$\mathbf{F}_{ij}^{\mathbf{y}}(\mathbf{\Phi}) = -\mathbb{E}_{[\mathbf{y};\,\mathbf{\Phi}|\mathbf{c}]}\big(\nabla_{\mathbf{\Phi}}\left[\nabla_{\mathbf{\Phi}} \log \Lambda(\mathbf{y};\mathbf{\Phi}|\mathbf{c})\right]\big), \tag{11}$$

where $\nabla_{\mathbf{\Phi}}$, is the first-order linear derivative and $\mathbb{E}[.]$ denotes the expectation operator. After evaluation of (11), we arrive at the following equation

$$\mathbf{F}_{ij}^{\mathbf{y}}(\mathbf{\Phi}) = \mathbf{F}_{ij}^{\Gamma\,(WIS)}(\mathbf{\Phi}) + \mathbf{F}_{ij}^{\Gamma\,(DS)} + \mathbf{F}_{ij}^{\Pi}(\mathbf{\Phi}) + \mathbf{F}_{ij}^{\Sigma}(\mathbf{\Phi}), \tag{12}$$

where $\mathbf{F}_{ij}^{\Gamma\,(WIS)}$ is calculated in Appendix 1 and is given as

$$\mathbf{F}_{ij}^{\Gamma\,(WIS)}(\mathbf{\Phi}) = \frac{8\pi^2(\Upsilon_{WIS})^2}{1+\Upsilon_{WIS}} \times \begin{bmatrix} \frac{1}{12\pi^2T^2}\left(\pi^2 + 3\alpha^2(\pi^2-8)\right) & 0 \\ 0 & \frac{T^2}{48\alpha}\left(3+4\alpha(N^2-1)\right) \end{bmatrix}, \tag{13}$$

$$\mathbf{F}_{ij}^{\Gamma\,(DS)}(\mathbf{\Phi}) = 2\kappa_{ij}\mathbf{F}_{ij}^{\Gamma\,(WIS)}(\mathbf{\Phi}), \tag{14}$$

$$\mathbf{F}_{ij}^{\Pi}(\mathbf{\Phi}) = \frac{-2\kappa_{ij}}{\Upsilon_{WIS}}\mathbf{F}_{ij}^{\Gamma\,(WIS)}(\mathbf{\Phi}), \tag{15}$$

$$\mathbf{F}_{ij}^{\Sigma}(\mathbf{\Phi}) = \frac{4\kappa_{ij}}{\Upsilon_{WIS}}\mathbf{F}_{ij}^{\Gamma\,(WIS)}(\mathbf{\Phi}). \tag{16}$$

Here $0 \leq \alpha \leq 1$ is a roll-off (excess bandwidth) factor. The first term is the contribution due to WIS and remaining terms are contribution due to DS, respectively. Our desired parameters of interest are the target's position and velocity components, i.e., $\mathbf{\Theta} = [p_x, p_y, p_z, v_x, v_y, v_z]$. The MFIM, i.e, $\mathbf{F}_{ij}(\mathbf{\Theta})$, is obtained by parameter transformation via using the chain rule as

$$\mathbf{F}_{ij}(\mathbf{\Theta}) = \left(\frac{\partial\mathbf{\Phi}}{\partial\mathbf{\Theta}}\right)\mathbf{F}_{ij}^{\mathbf{y}}(\mathbf{\Phi})\left(\frac{\partial\mathbf{\Phi}}{\partial\mathbf{\Theta}}\right)^T. \tag{17}$$

The entries of above transformation are given in Appendix 2. Here $\left(\frac{\partial\mathbf{\Phi}}{\partial\mathbf{\Theta}}\right) \in \mathbb{R}^{6\times 2}$ is the Jacobian matrix and its entries are calculated by taking the derivatives of the delay term in (4) and the Doppler term in (5) as in [8]. After all the calculations, the final expression for the required total MFIM over all transceiver pairs is given as

$$\mathbf{F}(\mathbf{\Theta}) = \frac{8\pi^2(\Upsilon_{WIS})}{1+\Upsilon_{WIS}} \sum_{i=1}^{M_T}\sum_{j=1}^{M_R}\mathbf{F}_{ij}(\mathbf{\Theta})(\Upsilon_{WIS} + 2(\Upsilon_{WIS})\kappa_{ij} + 2\kappa_{ij}), \tag{18}$$

where the parameter $\kappa_{ij} = |m_{ij}|^2/2\sigma^2$ is the Rician K factor and is the ratio of the power in DS to the power in WIS. Also, $\Upsilon_{WIS} = \sigma^2/\sigma_n^2$, is the SNR due to WIS. For Rician target, the total SNR $\Upsilon_{T_{ij}}$ is

$$\Upsilon_{T_{ij}} = \Upsilon_{WIS} + \Upsilon_{DS_{ij}}, \tag{19}$$

where $\Upsilon_{DS_{ij}} = |m_{ij}|^2/2\sigma_n^2$, is the SNR due to DS. We built a relationship of parameter κ_{ij} to another parameter κ'_{ij}, which is defined in [7] as $\kappa'_{ij} = \Upsilon_{DS_{ij}}/\Upsilon_{T_{ij}}$. After some algebraic manipulations it becomes

$$\kappa'_{ij} = \frac{\kappa_{ij}}{1+\kappa_{ij}}. \tag{20}$$

This parameter $0 \leq \kappa'_{ij} \leq 1$, is used for the classification of the target RCS models. For example, the Swerling-I/II models, Swerling-III/IV models and Swerling-$0/V$ models will correspond to the value of $\kappa'_{ij} = 0, 0.75$ and 1 in the probability density function given in [7]. From (18), it is evident that MFIM depends on various factors. It strongly depends on geometry which includes positions of transmitter,receiver and target with respect to each other and target velocity. Also it is strongly dependent on target RCS and SNR. Moreover, it also shows dependence on the waveform parameters such as RRC roll-off factor, symbol time and number of symbols. Finally, MCRLB is obtained by taking inverse of MFIM, i.e., $MCRLB = \mathbf{F}(\mathbf{\Theta})^{-1}$.

IV. Numerical Examples

TABLE I
POSITIONS OF TRANSMITTERS & RECEIVERS IN METERS

T_x	$[20, 25, 4]$	$[20, 30, 4]$	$[20, 35, 10]$	$[25, 22, 10]$	$[25, 28, 10]$
R_x	$[35, 5, 5]$	$[50, 5, 5]$	$[21, 10, 11]$	$[15, 15, 11]$	$[45, 41, 11]$

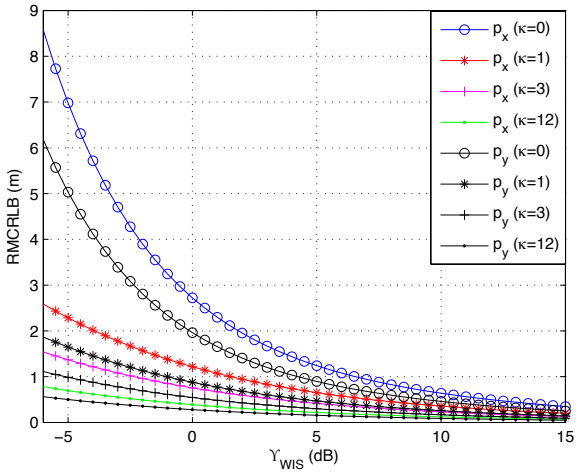

Fig. 1. RMCRLB for target position $(16, 26, 7)m$

For numerical evaluation, we consider five transmitters and five receivers, i.e., $M_T = 5 = M_R$, whose positions are given in Table I. By considering frequent WiFi beacon frame transmission, which is transmitted at a symbol rate of $1e^6$ symbols per second using BPSK modulation at channel 6. Here, we choose $f_c = 2.437GHz$, $T = 1\mu s$, $\alpha = 0.35$ and $NT = 0.4s$, which is considered reasonable for a slowly moving target. We consider two scenarios in which square roots of MCRLB (RMCRLBs) are plotted against Υ_{WIS}. In the first scenario, the effect of DS contribution on estimation

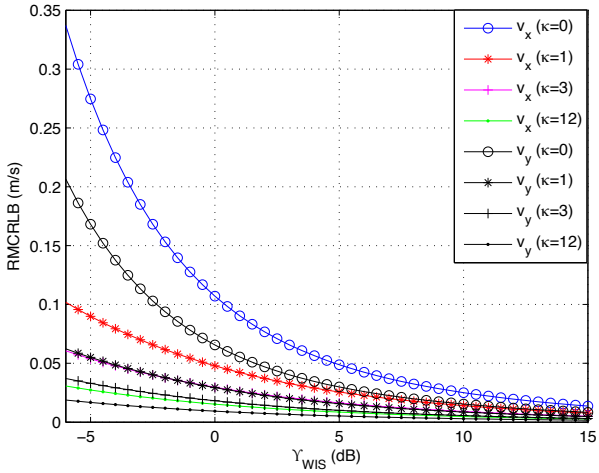

Fig. 2. RMCRLB for target velocity $(0.35, 0.15, 1.1)m/s$.

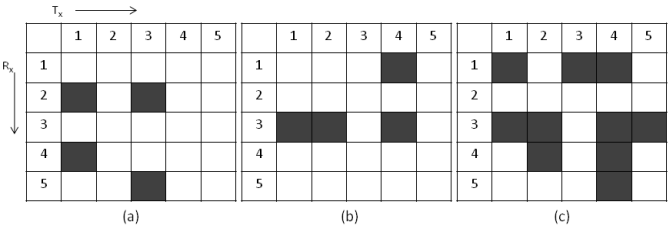

Fig. 3. Transceiver pairs selection with & without DS

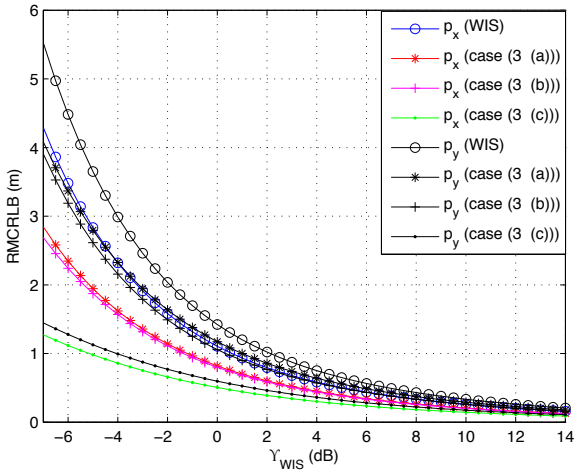

Fig. 4. RMCRLB for target position $(25, 15, 8)m$

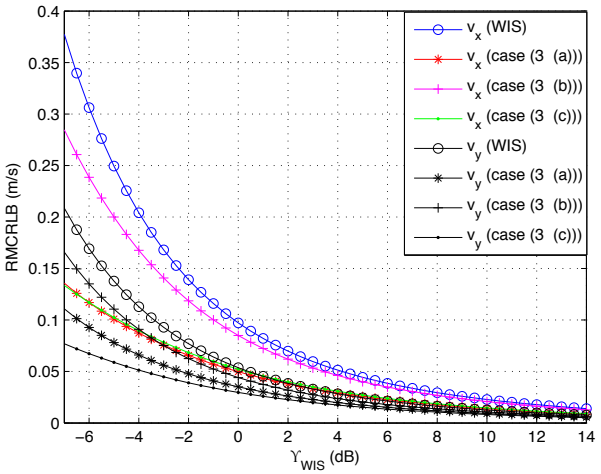

Fig. 5. RMCRLB for target velocity $(1.3, 0.3, 0.3)m/s$

accuracy is studied by varying κ_{ij}, where $\kappa_{ij} = \kappa$ is considered for all transceiver pairs without loss of generality. In this scenario, target is assumed at position $(16, 26, 7)m$ having typical human walking velocity of $1.164m/s$ with components $(0.35, 0.15, 1.1)m/s$.

From Figs. 1-2, it is obvious that RMCRLB decreases with increase in the value of κ. The reason is that with increase in κ, the target RCS increases, which results in increase in SNR at the receiver. Consequently, the estimation accuracy increases. Thus, the best estimation accuracy achieves for asymptotic limit $\kappa \to \infty$, however is generally not the case in indoor WiFi systems. In contrast, the estimation accuracy is worst when $\kappa = 0$ and target RCS follows Rayleigh fluctuations for all transceiver pairs

In practical situations, the DS may exist for a subset of transceiver pairs. In the second scenario, we analyze its effects along with the effect of geometry variation on the estimation accuracy. In Fig. 3, the existence and absence of DS for different transceiver pairs is shown, where the filled boxes show its presence and unfilled boxes show its absence. The target position and velocity are taken as $(25, 15, 8)m$ and $(1.3, 0.3, 0.3)m/s$, respectively. The Swerling-IV target is assumed by taking $\kappa = 3$ for transceiver pairs with DS. From Figs. 4-5, as the number of transceiver pairs with DS increases, the SNR increases and as a result estimation errors decrease. It is also seen that the choice of transceiver pair with DS is also important. For example, in Fig. 5 with equal number of transceiver pairs, the RMCRLB values of v_y at $-6dB$ for Fig. 3 (case (a)) and Fig. 3 (case (b)) are $0.1351m/s$ and $0.09281m/s$, respectively. This effect is attributed due to geometry. Also the Euclidean components of target position and velocity have different error (RMCRLB) values in scenario 1 than in scenario 2, due to change in the geometry. Also from scenario 2, performance limits are evaluated when target RCS appears different for transceiver pairs with and without DS component.

V. Conclusion

In this paper, the closed-form MCRLBs expressions are computed for a WiFi (802.11 b)-based passive multistatic radar operating in a RF environment. It is shown that total MFIM is the sum of MFIM due to both DS and WIS components. The MFIM is strongly dependent on geometry, SNR and type of target RCS besides dependence on waveform parameters. The

estimation accuracy increases with increase in DS contribution, SNR, number and/or choice of transceiver pairs. It is also shown that exploitation of DS can compensate the problem of low transmitting power. Furthermore, It is shown that using DS a waveform can be characterized for a range of target models, i.e., GRCSM appear in different radar applications. Also, the performance can be evaluated with different RCS characteristics of the target for different transceiver pairs.

APPENDIX 1

We now use equation (8), which gives

$$\Gamma_{ij} = \frac{\sigma^2}{\sigma_n^2+\sigma^2}\left|\int_{-\infty}^{\infty} y_{ij}(t)\overset{*}{u_i}(t-\tau_{ij})e^{-j2\pi f_{D_{ij}}(t-\tau_{ij})}dt\right|^2. \tag{21}$$

Suppose $\gamma_{ij} = \int_{-\infty}^{\infty} y_{ij}(t)\overset{*}{u_i}(t-\tau_{ij})e^{-j2\pi f_{D_{ij}}(t-\tau_{ij})}dt$, then from the above expression we determine the first derivative

$$\frac{\partial\Gamma_{ij}}{\partial\tau_{ij}} = \frac{\sigma^2}{\sigma_n^2+\sigma^2}\left(\frac{\partial\gamma_{ij}}{\partial\tau_{ij}}\overset{*}{\gamma_{ij}} + \gamma_{ij}\frac{\partial\overset{*}{\gamma_{ij}}}{\partial\tau_{ij}}\right). \tag{22}$$

The final expression after calculating all the derivatives of γ_{ij} and its conjugate, we obtain

$$\frac{\partial\Gamma_{ij}}{\partial\tau_{ij}} = \frac{2\sigma^2}{\sigma_n^2(\sigma_n^2+\sigma^2)}\Re\left(\gamma_{ij}\int_{-\infty}^{\infty}\overset{*}{y_{ij}}(t)\frac{\partial u_i}{\partial\tau_{ij}}e^{j2\pi f_{D_{ij}}(t-\tau_{ij})}dt\right). \tag{23}$$

From here onwards we omit the argument of $u_i(t-\tau_{ij})$, to reduce space. The second derivative with respect to τ_{ij}, after some simplifications becomes

$$\begin{aligned}\frac{\partial^2\Gamma_{ij}}{\partial\tau_{ij}^2} &= \frac{\sigma^2}{2(\sigma_n^2+\sigma^2)}\times\\ &\left\{\Re\left(\int_{-\infty}^{\infty} y_{ij}(t)\overset{*}{u_i}e^{-j2\pi f_{D_{ij}}(t-\tau_{ij})}dt\times\right.\right.\\ &\int_{-\infty}^{\infty}\overset{*}{y_{ij}}(t)\frac{\partial^2 u_i}{\partial\tau_{ij}^2}e^{j2\pi f_{D_{ij}}(t-\tau_{ij})}dt+\\ &\int_{-\infty}^{\infty}\overset{*}{y_{ij}}(t)\frac{\partial u_i}{\partial\tau_{ij}}e^{j2\pi f_{D_{ij}}(t-\tau_{ij})}dt\times\\ &\left.\left.\int_{-\infty}^{\infty} y_{ij}(t)\frac{\partial\overset{*}{u_i}}{\partial\tau_{ij}}e^{-j2\pi f_{D_{ij}}(t-\tau_{ij})}dt\right\}.\right.\end{aligned} \tag{24}$$

Now we take the expectation value while replacing the received signal from $y_{ij}(t)$ and using $\mathbb{E}[|\beta_{ij}|^2] = \sigma^2 + m_{ij}^2$, we arrive at the following equation

$$\begin{aligned}-\mathbb{E}\left(\frac{\partial^2\Gamma_{ij}}{\partial\tau_{ij}^2}\right) &= \frac{-2\sigma^2(\sigma^2+m_{ij}^2)}{(\sigma_n^2+\sigma^2)}\mathbb{E}\left\{\Re\left(\left|\int_{-\infty}^{\infty} u_i\frac{\partial\overset{*}{u_i}}{\partial\tau_{ij}}dt\right|^2+\right.\right.\\ &\left.\left.\int_{-\infty}^{\infty}|u_i|^2dt\int_{-\infty}^{\infty}\overset{*}{u_i}\frac{\partial^2 u_i}{\partial\tau_{ij}^2}dt\right)\right\}.\end{aligned} \tag{25}$$

Now the derivative of u_i, is an odd function therefore the integrand of the first integral is an odd function, which makes it zero. On the other hand, the second term can be simplified into

$$\begin{aligned}&\int_{-\infty}^{\infty}\overset{*}{u_i}\frac{\partial^2 u_i}{\partial\tau_{ij}^2}dt = \frac{1}{N^2}\sum_{k=0}^{N-1}\sum_{n=0}^{N-1}\overset{*}{c_{ik}}c_{in}\\ &\int_{-\infty}^{\infty}\overset{*}{h_i}\left(t-\tau_{ij}-kT-\frac{D}{2}\right)\frac{\partial^2 h_i\left(t-\tau_{ij}-nT-\frac{D}{2}\right)}{\partial\tau_{ij}^2}dt,\end{aligned} \tag{26}$$

where we have used the normalization condition $\int_{-\infty}^{\infty}|u_i|^2dt = 1$. By using the expectation condition and (2) we obtain

$$-\mathbb{E}\left(\frac{\partial^2\Gamma_{ij}}{\partial\tau_{ij}^2}\right) = \frac{-2\sigma^2(\sigma^2+m_{ij}^2)}{(\sigma_n^2+\sigma^2)}\left\{\int_{-\infty}^{\infty}\overset{*}{h_i}(t)\frac{\partial^2 h_i(t)}{\partial t^2}dt\right\}. \tag{27}$$

The above integral is already evaluated in [10], hence we get

$$-\mathbb{E}\left(\frac{\partial^2\Gamma_{ij}}{\partial\tau_{ij}^2}\right) = \frac{2\sigma^2(\sigma^2+|m_{ij}|^2)}{3T^2\sigma_n^2(\sigma_n^2+\sigma^2)}\left(\pi^2+3\alpha^2(\pi^2-8)\right). \tag{28}$$

Finally, we write the above expression in terms of the SNR

$$-\mathbb{E}\left(\frac{\partial^2\Gamma_{ij}}{\partial\tau_{ij}^2}\right) = \frac{2(\Upsilon_{WIS})^2(1+2\kappa_{ij})}{3T^2(1+\Upsilon_{WIS})}\left(\pi^2+3\alpha^2(\pi^2-8)\right), \tag{29}$$

using $\kappa_{ij} = |m_{ij}|/2\sigma^2$ and $\Upsilon_{WIS} = \sigma^2/\sigma_n^2$. To compute the expectation with respect to other second-order derivatives, we follow the same procedure and arrive at the following closed-form expression

$$-\mathbb{E}\left(\frac{\partial^2\Gamma_{ij}}{\partial f_{D_{ij}}^2}\right) = \frac{\pi^2T^2(\Upsilon_{WIS})^2(1+2\kappa_{ij})}{6\alpha(1+\Upsilon_{WIS})}\left(3+4\alpha(N^2-1)\right). \tag{30}$$

All off-diagonal terms turn out to be zero in agreement with the calculations in [10]. Following the same lines, we obtain the expectation of second-order derivatives of Π_{ij} terms. By using (8), the first-derivative of Π_{ij}, is given by

$$\begin{aligned}\frac{\partial\Pi_{ij}}{\partial\tau_{ij}} &= \frac{2}{(\sigma_n^2+\sigma^2)}\Re\left(\int_{-\infty}^{\infty} m_{y_{ij}}\overset{*}{u_i}(t-\tau_{ij})\mathrm{e}^{-j2\pi f_{D_{ij}}(t-\tau_{ij})}dt\right.\\ &\left.\int_{-\infty}^{\infty} m_{y_{ij}}^*\frac{\partial u_i}{\partial\tau_{ij}}e^{j2\pi f_{D_{ij}}(t-\tau_{ij})}dt\right),\end{aligned} \tag{31}$$

whose second derivative after taking the expectation takes the form

$$
\begin{aligned}
-\mathbb{E}\left(\frac{\partial^2\Pi_{ij}}{\partial\tau_{ij}^2}\right) &= \frac{-2}{(\sigma_n^2+\sigma^2)}\times \\
&\mathbb{E}\Bigg\{\Re\Bigg(\int_{-\infty}^{\infty} m_{y_{ij}}\overset{*}{u}_i e^{-j2\pi f_{D_{ij}}(t-\tau_{ij})}dt\times \\
&\Bigg(\int_{-\infty}^{\infty} m^*_{y_{ij}}\frac{\partial^2 u_i}{\partial\tau_{ij}^2}e^{j2\pi f_{D_{ij}}(t-\tau_{ij})}dt+ \\
&\int_{-\infty}^{\infty} m^*_{y_{ij}}\frac{\partial u_i}{\partial\tau_{ij}}e^{j2\pi f_{D_{ij}}(t-\tau_{ij})}dt\times \\
&\Bigg(\int_{-\infty}^{\infty} m_{y_{ij}}\frac{\partial \overset{*}{u}_i}{\partial\tau_{ij}}e^{-j2\pi f_{D_{ij}}(t-\tau_{ij})}dt\Bigg)\Bigg)\Bigg\}. \qquad (32)
\end{aligned}
$$

Now after substituting the value of $m_{y_{ij}}$, i.e., ($m_{y_{ij}} = m_{ij}u_i\, e^{j2\pi f_{D_{ij}}(t-\tau_{ij})}$), and using the fact that the integral of an odd function is zero, it is easy to see that the second term in the above equation is zero while the first term reduces to

$$
-\mathbb{E}\left(\frac{\partial^2\Pi_{ij}}{\partial\tau_{ij}^2}\right) = \frac{-2|m_{ij}|^2}{(\sigma_n^2+\sigma^2)}\,\mathbb{E}\Bigg\{\Re\Bigg(\int_{-\infty}^{\infty}\overset{*}{u}_i\frac{\partial^2 u_i}{\partial\tau_{ij}^2}dt\Bigg)\Bigg\}, \quad (33)
$$

which finally gives

$$
-\mathbb{E}\left(\frac{\partial^2\Pi_{ij}}{\partial\tau_{ij}^2}\right) = \frac{2(\Upsilon_{WIS})\kappa_{ij}}{3T^2(1+\Upsilon_{WIS})}\big(\pi^2+3\alpha^2(\pi^2-8)\big). \quad (34)
$$

For the rest of the terms it can be shown that

$$
-\mathbb{E}\left(\frac{\partial^2\Pi_{ij}}{\partial f_{D_{ij}}^2}\right) = \frac{\pi^2T^2(\Upsilon_{WIS})\kappa_{ij}}{6\alpha(1+\Upsilon_{WIS})}\big(3+4\alpha(N^2-1)\big), \quad (35)
$$

$$
-\mathbb{E}\left(\frac{\partial^2\Sigma_{ij}}{\partial\tau_{ij}^2}\right) = \frac{4(\Upsilon_{WIS})\kappa_{ij}\big(\pi^2+3\alpha^2(\pi^2-8)\big)}{3T^2(1+\Upsilon_{WIS})}, \quad (36)
$$

$$
-\mathbb{E}\left(\frac{\partial^2\Sigma_{ij}}{\partial f_{D_{ij}}^2}\right) = \frac{\pi^2T^2(\Upsilon_{WIS})\kappa_{ij}\big(3+4\alpha(N^2-1)\big)}{3\alpha(1+\Upsilon_{WIS})}. \quad (37)
$$

APPENDIX 2

The Entries of MFIM $\mathbf{F}_{ij}(\mathbf{\Theta})$

Since the MFIM on parameter, $\Phi = [\tau_{ij}, f_{D_{ij}}]$ is only a diagonal matrix of order 2×2, we denote it by $\mathbf{F}_{ij}(\mathbf{\Phi}) = \text{diag}[F^{11}, F^{22}]$. Now the required MFIM $\mathbf{F}_{ij}(\mathbf{\Theta})$ is a 6×6 symmetric matrix which arises on the parameters of interest and it depends more on the geometry due to presence of the Jacobian rather than $\mathbf{F}_{ij}(\mathbf{\Phi})$. Thus we obtain the following entries of MFIM $\mathbf{F}_{ij}(\mathbf{\Theta})$.

$$
\begin{aligned}
\mathbf{F}_{ij}^{11}(\mathbf{\Theta}) &= (\tau_{ij,p_x})^2F^{11} + (f_{D_{ij,p_x}})^2F^{22},\\
\mathbf{F}_{ij}^{12}(\mathbf{\Theta}) &= (\tau_{ij,p_x})(\tau_{ij,p_y})F^{11} + (f_{D_{ij,p_x}})(f_{D_{ij,p_y}})F^{22},\\
\mathbf{F}_{ij}^{13}(\mathbf{\Theta}) &= (\tau_{ij,p_x})(\tau_{ij,p_z})F^{11} + (f_{D_{ij,p_x}})(f_{D_{ij,p_z}})F^{22},\\
\mathbf{F}_{ij}^{14}(\mathbf{\Theta}) &= (f_{D_{ij,p_x}})(f_{D_{ij,v_x}})F^{22},\\
\mathbf{F}_{ij}^{15}(\mathbf{\Theta}) &= (f_{D_{ij,p_x}})(f_{D_{ij,v_y}})F^{22},\\
\mathbf{F}_{ij}^{16}(\mathbf{\Theta}) &= (f_{D_{ij,p_x}})(f_{D_{ij,v_z}})F^{22},\\
\mathbf{F}_{ij}^{22}(\mathbf{\Theta}) &= (\tau_{ij,p_y})^2F^{11} + (f_{D_{ij,p_y}})^2F^{22},\\
\mathbf{F}_{ij}^{23}(\mathbf{\Theta}) &= (\tau_{ij,p_y})(\tau_{ij,p_z})F^{11} + (f_{D_{ij,p_y}})(f_{D_{ij,p_z}})F^{22},\\
\mathbf{F}_{ij}^{24}(\mathbf{\Theta}) &= (f_{D_{ij,p_y}})(f_{D_{ij,v_x}})F^{22},\\
\mathbf{F}_{ij}^{25}(\mathbf{\Theta}) &= (f_{D_{ij,p_y}})(f_{D_{ij,v_y}})F^{22},\\
\mathbf{F}_{ij}^{26}(\mathbf{\Theta}) &= (f_{D_{ij,p_y}})(f_{D_{ij,v_z}})F^{22},\\
\mathbf{F}_{ij}^{33}(\mathbf{\Theta}) &= (\tau_{ij},p_z)^2F^{11} + (f_{D_{ij,p_z}})^2F^{22},\\
\mathbf{F}_{ij}^{34}(\mathbf{\Theta}) &= (f_{D_{ij,p_z}})(f_{D_{ij,v_x}})F^{22},\\
\mathbf{F}_{ij}^{35}(\mathbf{\Theta}) &= (f_{D_{ij,p_z}})(f_{D_{ij,v_y}})F^{22},\\
\mathbf{F}_{ij}^{36}(\mathbf{\Theta}) &= (f_{D_{ij,p_z}})(f_{D_{ij,v_z}})F^{22},\\
\mathbf{F}_{ij}^{44}(\mathbf{\Theta}) &= (f_{D_{ij,v_x}})^2F^{22},\\
\mathbf{F}_{ij}^{45}(\mathbf{\Theta}) &= (f_{D_{ij,v_x}})(f_{D_{ij,v_y}})F^{22},\\
\mathbf{F}_{ij}^{46}(\mathbf{\Theta}) &= (f_{ij,v_x})(f_{ij,v_z})F^{22},\\
\mathbf{F}_{ij}^{55}(\mathbf{\Theta}) &= (f_{D_{ij,v_y}})^2F^{22},\\
\mathbf{F}_{ij}^{56}(\mathbf{\Theta}) &= (f_{D_{ij,v_y}})(f_{D_{ij,v_z}})F^{22},\\
\mathbf{F}_{ij}^{66}(\mathbf{\Theta}) &= (f_{D_{ij,v_z}})^2F^{22}.
\end{aligned}
$$

REFERENCES

[1] H. Griffiths, "Passive bistatic radar and waveform diversity," Tech. Rep., *DTIC Document*, 2009.

[2] D. Pastina, F. Colone, T. Martellis, P. Falcone, "Parasitic exploitation of Wi-Fi Signals for indoor radar surveillance," *IEEE Trans. Veh. Technol.*, vol. 64, no. 4, pp. 1401-1415, 2015.

[3] P. Falcone, F. Colone, C. Bongioanni, P. Lombardo, "Experimental results for OFDM WiFi-based passive bistatic radar," *IEEE Radar Conf.*, pp. 516-521, 2010.

[4] P. Falcone, F. Colone, P. Lombardo, "Potentialities and challenges of WiFi-based passive radar," *IEEE Aerospace and Electronic Systems Magazine*, vol. 27, no. 11, pp. 15-26, 2012.

[5] H. Mazhar, S. A. Hassan, "Analysis of target multipaths in WiFi-based passive radars," *IET Radar, Sonar & Navigation*, vol. 10, no. 1, pp. 140-145, Jan. 2016.

[6] Z. Zhou, et al., "WiFi-Based indoor line-of-sight identification," *IEEE Trans. Wireless Communications*, vol.14, no. 11, pp. 6125-6136, 2015.

[7] C. D. Papanicolopoulos, W. D. Blair, D. L. Sherman, and M. Brandt-Pearce,"Use of a Rician distribution for modeling aspect-dependent RCS amplitude and scintillation," *IEEE Radar Conf. (RADAR)*, pp. 218–223, 2007.

[8] S. Gogineni, M. Rangaswamy, B. D. Rigling, and A. Nehorai, "Cramér-Rao bounds for UMTS-based passive multistatic radar," *IEEE Trans. Signal Processing*, vol. 62, no. 1, pp. 95–106, 2014.

[9] H. L. V. Trees, *Detection, Estimation, and Modulation Theory III*, John Wiley & Sons, 2001.

[10] P. Stinco, M. S. Greco, F. Gini, and M. Rangaswamy, "Ambiguity function and Cramér–Rao bounds for universal mobile telecommunications system-based passive coherent location systems," *IET Radar, Sonar & Navigation*, vol. 6, no. 7, pp. 668-678, 2012.